Theoretical and Experimental Analysis on InAlGaAs/AlGaAs Active Region of 850-nm Vertical-Cavity Surface-Emitting Lasers

Yi-An Chang, Jun-Rong Chen, Hao-Chung Kuo, *Member, IEEE*, Yen-Kuang Kuo, and Shing-Chung Wang, *Senior Member, IEEE*, *Fellow, OSA*

***Abstract*—In this study, the gain-carrier characteristics of $In_{0.02}Ga_{0.98}As$ and InAlGaAs quantum wells (QWs) of variant In and Al compositions with an emission wavelength of 838 nm are theoretically investigated. More compressive strain, caused by higher In and Al compositions in InAlGaAs QW, is found to provide higher material gain, lower transparency carrier concentration, and transparency radiative current density over the temperature range of 25–95 °C. To improve the output characteristics and high-temperature performance of 850-nm vertical-cavity surface-emitting laser (VCSEL), $In_{0.15}Al_{0.08}Ga_{0.77}As/Al_{0.3}Ga_{0.7}As$ is utilized as the active region, and a high-bandgap 10-nm-thick $Al_{0.75}Ga_{0.25}As$ electronic blocking layer is employed for the first time. The threshold current and slope efficiency of the VCSEL with $Al_{0.75}Ga_{0.25}As$ at 25 °C are 1.33 mA and 0.53 W/A, respectively. When this VCSEL is operated at an elevated temperature of 95 °C, the increase in threshold current is less than 21% and the decrease in slope efficiency is approximately 24.5%. A modulation bandwidth of 9.2 GHz biased at 4 mA is demonstrated.**

***Index Terms*—Electronic blocking layer, gain modeling, InAlGaAs/AlGaAs, MOCVD, semiconductor lasers, 850-nm VCSEL.**

I. Introduction

VERTICAL-CAVITY surface-emitting lasers (VCSELs) with 850-nm emission had become standard in local area interconnects and free-space optical communications. The advantages, including relatively low threshold current, low divergent angle, and circular beam, which lead to simpler packaging, of these surface emission devices had been found to provide the low-cost short-distance data links [1]–[4]. To emit at 850 nm, the choice of the active region grown on GaAs substrate had been conscious of the materials including (In)GaAs/AlGaAs [5], [6], InAlGaAs/AlGaAs [7]–[9], and InGaAsP/InGaP [10], [11]. The incorporation of In into GaAs quantum wells (QWs) had been demonstrated to provide compressive strain, which, in turn, resulted in lower threshold current and higher modulation speed [12], [13]. Previous research also showed that the InGaAsP, which was used during most of the initial development of long-wavelength VCSELs, could provide comparable laser performance [5], [14]–[16].

It is well known that low transparency current achievable with strained QWs is required for providing low threshold current in a semiconductor laser. For laser devices with an emission wavelength of 850 nm, the incorporation of Al into InGaAs QWs with higher In composition can possess a desired strain level that beneficially reduces the threshold current densities of the devices [17], [18]. However, qualitative analysis of varying Al and In contents in approximately 850 nm InAlGaAs QWs is rarely reported in literature. In this study, we first theoretically study the gain-carrier characteristics of InGaAs and InAlGaAs QWs with variant In and Al compositions in order to investigate the In and Al compositional effect in InAlGaAs QWs. Then, an InAlGaAs QW is prepared by metal–organic chemical vapor deposition (MOCVD), and the optical properties are studied by temperature dependent photoluminescence (PL). The device characteristics of 850-nm InAlGaAs/AlGaAs VCSELs are then investigated. To improve the high-temperature performance, we propose to incorporate a high-bandgap 10-nm-thick $Al_{0.75}Ga_{0.25}As$ electronic blocking layer into the InAlGaAs/AlGaAs VCSELs for the first time. The threshold current and slope efficiency of the devices with a high-bandgap 10-nm-thick $Al_{0.75}Ga_{0.25}As$ electronic blocking layer are found to be less sensitive to the substrate temperature, and the output performance is enhanced in the mean time.

II. Physical Model and QW Optical Characteristics

For the InGaAs QWs and InAlGaAs QWs with variant In and Al compositions, the gain spectra and optical gain as a function of carrier density were calculated using the $k \cdot p$ theory with valence band mixing effects. An 8×8 Luttinger–Kohn Hamiltonian matrix with imposing an envelope function approximation was utilized in this investigation. The methods were closely followed by Chuang [19]. In the case of valence mixing, the valence bands are not parabolic and the gain spectrum can be expressed in numerical integration over k_t as

$$g(E) = \frac{g_0}{2\pi t E} \sum_{i,j} \int_0^\infty \frac{\left(\frac{\pi}{\Gamma}\right) f_{dip}(k_t) M_b (f_j - f_i)\, dk_t^2}{1 + \frac{(E_{cj}(k_t) - E_{kpi}(k_t) - E)^2}{\Gamma^2}} \qquad (1)$$

Manuscript received April 26, 2005; revised September 1, 2005. This work was supported by the National Science Council, China, under Grants NSC-93-2120-M009-006 and NSC-93-2112-M-018-008, and by the Academic Excellence Program of the Ministry of Education of China under Contract NSC-93-2752-E009-008.

Y.-A. Chang, H.-C. Kuo, and S.-C. Wang are with the Institute of Electro-Optical Engineering, National Chiao-Tung University, Hsinchu 30036, Taiwan, R.O.C. (e-mail: rayman0313.eo92g@nctu.edu.tw; hckuo@faculty.nctu.edu.tw; scwang@cc.nctu.edu.tw).

J.-R. Chen and Y.-K. Kuo are with the Department of Physics, National Changhua University of Education, Changhua 50058, Taiwan, R.O.C. (e-mail: hahahasrc@yahoo.com.tw; ykuo@cc.ncue.edu.tw).

Digital Object Identifier 10.1109/JLT.2005.860156

where t is the thickness of QW, $\Gamma = \hbar/\tau_{\rm scat}$ is the broadening due to intraband scattering relaxation time $\tau_{\rm scat}$, E_{cj} is the jth conduction subband, and E_{kpi} is the ith valence subband from the $k \cdot p$ calculation. The sum is over all possible conduction and valence subbands. $g_0 = \pi q^2 \hbar/\varepsilon_0 c m_0^2 n$ is constant, with all symbols having their usual meanings. M_b is the dipole moment given by

$$M_b = \frac{1}{6} \cdot \frac{m_0 q}{m_c} \cdot \frac{E_{g0}(E_{g0} + \Delta_{\rm so})}{E_{g0} + \frac{2\Delta_{\rm so}}{3}} \tag{2}$$

where E_{g0} is the unstrained energy bandgap, m_c is the effective mass of the conduction band, and $\Delta_{\rm so}$ is the spin–orbit coupling energy. The error in the calculation of the Fermi functions, which are approximated with linear combinations of four exponential terms, is less than 0.04%, and that in the determination of the eigenvalues in the QW is less than 2×10^{-6}.

All the well widths of InGaAs and InAlGaAs QWs are designed to be 7 nm. Numerical parameters, required for the $k \cdot p$ theory, used in this calculation, are taken from [20]. The energy bandgaps of binary InAs, AlAs, and GaAs alloys at 25 °C are 0.354, 3.004, 1.423 eV, respectively, and the temperature-dependent energy bandgaps are governed by the Varshini equation. Specifically, the temperature-dependent energy bandgaps of the binary alloys are calculated by

$$E_g(\text{InAs}) = 0.417 - \frac{0.276 \times 10^{-3} \cdot T^2}{T + 93} \tag{3}$$

$$E_g(\text{AlAs}) = 3.099 - \frac{0.885 \times 10^{-3} \cdot T^2}{T + 530} \tag{4}$$

$$E_g(\text{GaAs}) = 1.519 - \frac{0.5405 \times 10^{-3} \cdot T^2}{T + 204}. \tag{5}$$

For the energy bandgaps of ternary GaInAs, AlInAs, and GaAlAs, and quaternary InAlGaAs alloys, the interpolation formulas are adapted from the composition-dependent properties [21]

$$E_g^{\alpha}(\text{AlGaAs}) = \alpha \cdot E_g(\text{AlAs}) + (1-\alpha) \cdot E_g(\text{GaAs}) - \alpha(1-\alpha) \cdot b\_\text{GaAlAs} \tag{6}$$

$$E_g^{\beta}(\text{AlInAs}) = \beta \cdot E_g(\text{InAs}) + (1-\beta) \cdot E_g(\text{AlAs}) - \beta \cdot (1-\beta) \cdot b\_\text{AlInAs} \tag{7}$$

$$E_g^{\gamma}(\text{GaInAs}) = \gamma \cdot E_g(\text{InAs}) + (1-\gamma) \cdot E_g(\text{GaAs}) - \gamma \cdot (1-\gamma) \cdot b\_\text{GaInAs} \tag{8}$$

$$E_g(\text{GaAlInAs}) = \frac{xw \cdot yw \cdot E_g^{\alpha}(\text{AlGaAs})}{xw \cdot yw + yw \cdot zw + zw \cdot xw} + \frac{yw \cdot zw \cdot E_g^{\beta}(\text{AlInAs})}{xw \cdot yw + yw \cdot zw + zw \cdot xw} + \frac{xw \cdot zw \cdot E_g^{\gamma}(\text{GaInAs})}{xw \cdot yw + yw \cdot zw + zw \cdot xw} \tag{9}$$

$$\alpha = \frac{1 - xw + yw}{2}$$

$$\beta = \frac{1 - yw + zw}{2}$$

$$\gamma = \frac{1 - xw + zw}{2} \tag{10}$$

where xw, yw, and zw represent the Ga, Al, and In compositions in InAlGaAsQW, respectively, and

$$b\_\text{GaAlAs} = -0.127 + 1.310 \cdot yw \tag{11}$$

$$b\_\text{AlInAs} = 0.7 \tag{12}$$

$$b\_\text{GaInAs} = 0.477. \tag{13}$$

The spontaneous emission rate is calculated by

$$\gamma_{\rm sp}^{\rm qw}(E) = \sum_{ij} \left(\frac{2\pi}{\hbar}\right) |H_{ij}|^2 f_j(1-f_i) D(E) \rho_{ij} \tag{14}$$

where

$$|H_{ij}|^2 = \left(\frac{q}{m_0}\right)^2 \left(\frac{2\hbar w}{4\varepsilon_1 \varepsilon_0 \omega^2}\right) M_{ij}^2 \tag{15}$$

$$\rho_{ij} = \rho_{ij}^0 \cdot h\left(\hbar\omega - E_{ij}^0\right) \tag{16}$$

and f_i and f_j represent the Fermi functions for the ith and jth levels, respectively. $D(E)$ is the optical mode density.

For a fixed QW emission wavelength of 838 nm, the In composition in InGaAs QW is theoretically determined to be 2%, and a series design of InAlGaAs QWs with various In and Al compositions of (In, Al) = (8.5%, 4%), (15%, 8%), (21%, 12%), and (27%, 16%) is performed with unchanged $Al_{0.3}Ga_{0.7}As$ barriers. The induced compressive strains in $In_{0.02}Ga_{0.98}As$, $In_{0.085}Al_{0.04}Ga_{0.875}As$, $In_{0.15}Al_{0.08}Ga_{0.77}As$, $In_{0.21}Al_{0.12}Ga_{0.67}As$, and $In_{0.27}Al_{0.16}Ga_{0.57}As$ QWs are 0.143%, 0.611%, 1.053%, 1.498%, and 1.918%, respectively.

The material gain available from a QW can be affected by a number of factors that need to be taken into account. It is well known that the QWs have to be designed with a low density of states and a closely matched density of states in the valence and conduction bands [22]–[24]. However, a low density of states will cause the rapid rising of Fermi level with increased temperature; that is, more carriers may escape from the QW at elevated temperatures. Therefore, a large conduction band offset is required to secure the carrier confinement. Fig. 1 shows the calculated material gains of the $In_{0.02}Ga_{0.98}As$ and InAlGaAs QWs with $Al_{0.3}Ga_{0.7}As$ barrier at 25 °C when the input carrier concentration is 6×10^{18} cm^{-3}. The InAlGaAs QWs with variant Al compositions of 4%, 8%, 12%, and 16% are calculated and compared with the $In_{0.02}Ga_{0.98}As$ QW. In the calculation of the radiative currents, the thickness of the AlGaAs barriers is assumed to be three times that of the QWs. Moreover, the material of the barriers is $Al_{0.3}Ga_{0.7}As$ throughout the numerical analysis. It is found that the InAlGaAs QWs can provide higher material gain than the $In_{0.02}Ga_{0.98}As$ QW. It is also noteworthy that the material gain of the InAlGaAs QWs can be enhanced when the Al composition in InAlGaAs

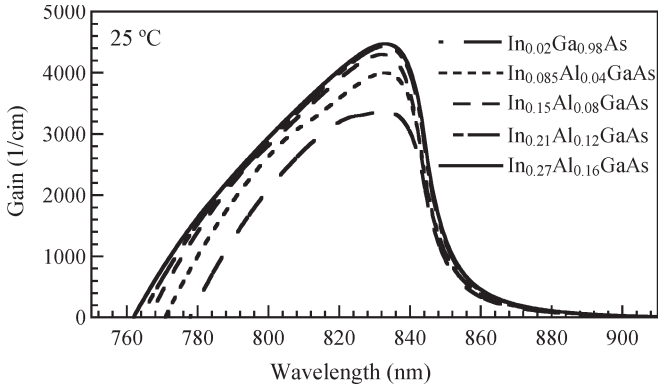

Fig. 1. Calculated material gains of the $In_{0.02}Ga_{0.98}As$ and InAlGaAs QWs with $Al_{0.3}Ga_{0.7}As$ barrier at 25 °C when the input carrier concentration is 6×10^{18} cm^{-3}. The material gain tends to saturate when the Al composition in InAlGaAs QW is higher than 8%.

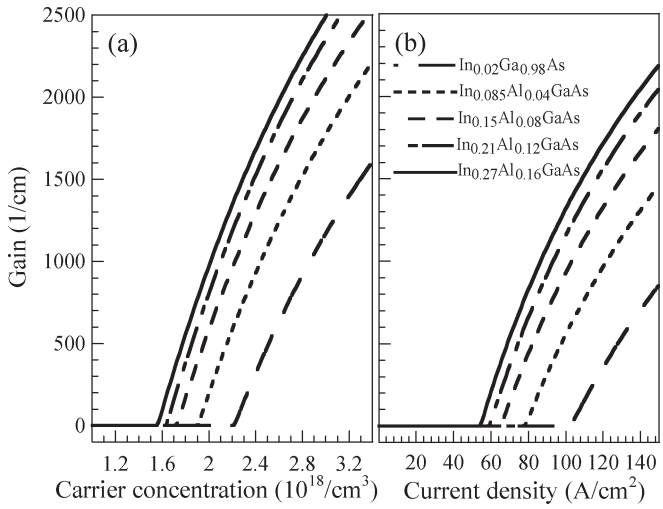

Fig. 2. Peak material gain as a function of (a) carrier concentration and (b) radiative current density of the $In_{0.02}Ga_{0.98}As$ and InAlGaAs QWs with $Al_{0.3}Ga_{0.7}As$ barrier at 25 °C.

QW is increased. The material gain tends to saturate when the Al composition in InAlGaAs QW is higher than 8%.

Fig. 2 shows the peak material gain as a function of (a) carrier concentration and (b) radiative current density of the $In_{0.02}Ga_{0.98}As$ and InAlGaAs QWs with $Al_{0.3}Ga_{0.7}As$ barrier at 25 °C. The radiative current density is obtained from the integral of spontaneous emission spectrum and the thickness of QW [25], [26]. Both the transparencies of carrier concentration and radiative current density of the InAlGaAs QWs are lower than those of the $In_{0.02}Ga_{0.98}As$ QW. The transparency carrier concentration depends primarily on the band curvatures, which is sensitive to the effective masses and the amount of strain. When the Al composition in InAlGaAs QW increases with increased In composition, the transparency carrier concentration decreases. Numerical results indicate that the density of states and the effective mass decrease with increased Al composition in InAlGaAs QW. The decrement in transparency carrier concentration is less apparent when the Al composition is higher than 8%.

Fig. 3 shows the curves of valence band for the $In_{0.02}Ga_{0.98}As$ and InAlGaAs QWs with variant In and Al compositions at 25 °C. The y axis of the figures represents the valence band QW potential. It is found that there are four confined hole levels in the InAlGaAs QWs, and the $In_{0.02}Ga_{0.98}As$ QW has another confined hole level (LH_2) in addition to the four HH_1, HH_2, LH_1, and HH_3 confined levels. The number of confined hole levels may be influenced by the amount of strain in QWs and the effective masses of electrons and holes. With the increase of In and Al compositions in InAlGaAs QW, the amount of strain in QWs increases, and the effective mass of holes decreases. The reduction of the density of states in the valence band is desirous, because low transparency carrier concentration can be achieved.

When the QW is at a temperature of 95 °C, the spectra of material gain and the peak material gain as a function of carrier concentration and radiative current density of the $In_{0.02}Ga_{0.98}As$ and InAlGaAs QWs with $Al_{0.3}Ga_{0.7}As$ barrier are shown in Figs. 4, and 5, respectively. The InAlGaAs QW with more In and Al compositions is also found to provide higher material gain, and the gain tends to saturate when the Al composition is higher than 12%. The red shift of the peak emission wavelength is 0.25 nm/K, which is approximately the same for all $In_{0.02}Ga_{0.98}As$ and InAlGaAs QWs. The decrement of the peak material gain with increased temperature from 25 to 95 °C in $In_{0.02}Ga_{0.98}As$ and InAlGaAs QWs is also approximately the same when the input carrier concentration remains unchanged at 6×10^{18} cm^{-3}. As indicated in Fig. 5, lower transparency carrier concentration and radiative current density are observed when the In and Al compositions in InAlGaAs QW increase. Due to the relatively incremental compressive strain, higher differential gain is also obtained over the temperature range under study. In this study, it is prognosticated that the transparency carrier concentration of the $In_{0.02}Ga_{0.98}As$ QW is increased by approximately 26.8% as temperature increases from 25 to 95 °C. For InAlGaAs QWs, the transparency carrier concentrations are increased by 26.3% (Al = 4%), 25.2% (Al = 8%), 23.8% (Al = 12%) and 21.7% (Al = 16%) as temperature increases from 25 to 95 °C, which are smaller than those of the $In_{0.02}Ga_{0.98}As$ QWs, because more compressive strain in QW can reduce the transparency carrier concentration and the relatively large conduction band offset, which is increased with the increase of In and Al compositions in InAlGaAs QW, can prevent carriers from escaping from the QW. In addition, the increase of transparency carrier concentration with increased temperature is attributed to the increment of nonradiative recombination and the poor electron confinement; namely, large amount of electrons can pile up from the QW and overflow without attributing to the radiative recombination, when the temperature is high.

III. Optical Property of QW and Device Fabrication

After investigating the numerical gain-carrier characteristics of the $In_{0.02}Ga_{0.98}As$ and InAlGaAs QWs, the next step is to fabricate the 850-nm VCSELs. The numerical results suggest that the InAlGaAs QWs with Al composition higher than 8% can provide better gain–carrier characteristics. However, although crystal quality concerns cannot be taken into account

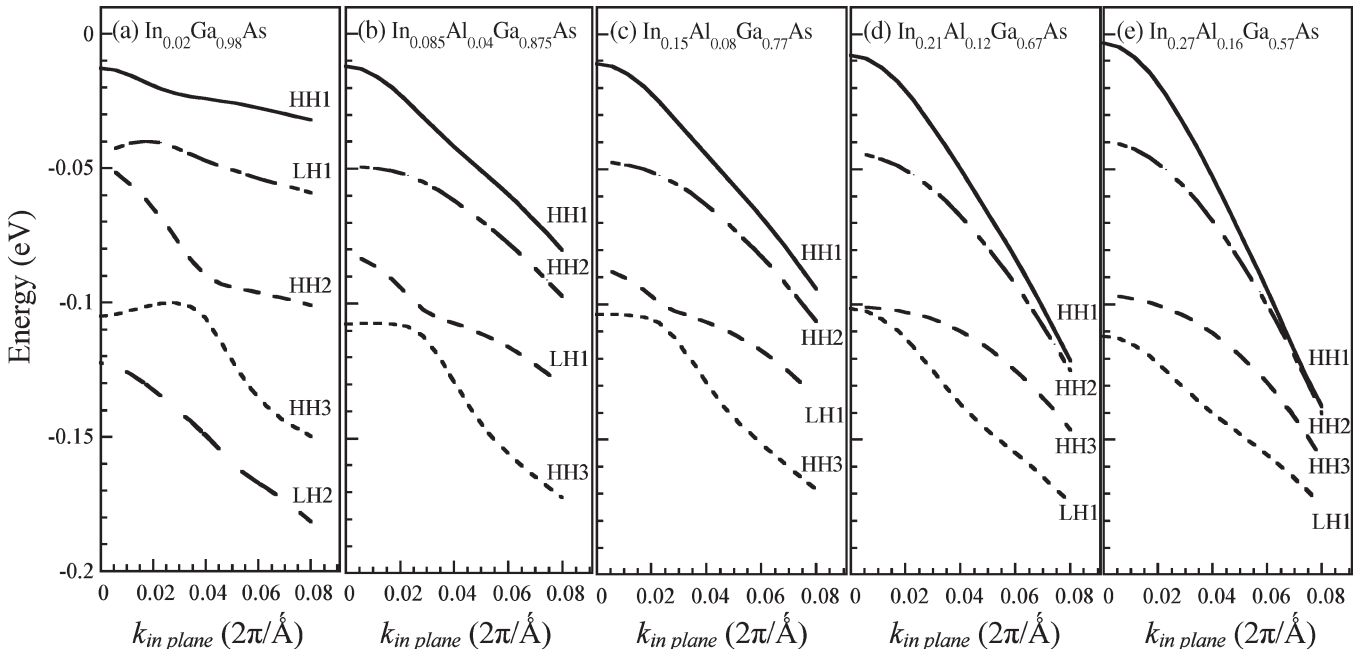

Fig. 3. Curves of valence band for the $In_{0.02}Ga_{0.98}As$ and InAlGaAs QWs with variant In and Al compositions at 25 °C. The y-axis of the figures represents the valence band QW potential.

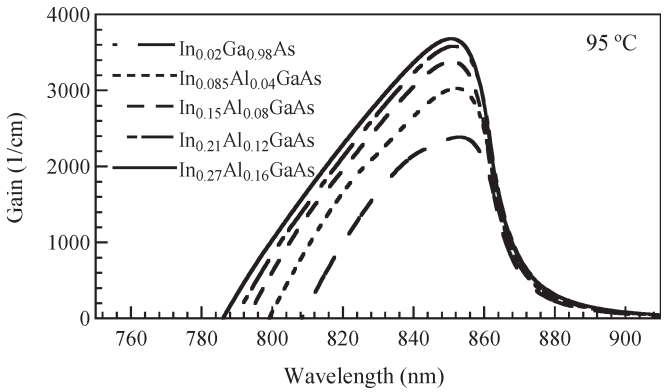

Fig. 4. Calculated spectra of material gains of the $In_{0.02}Ga_{0.98}As$ and InAlGaAs QWs with $Al_{0.3}Ga_{0.7}As$ barrier at 95 °C when the input carrier concentration is 6×10^{18} cm^{-3}.

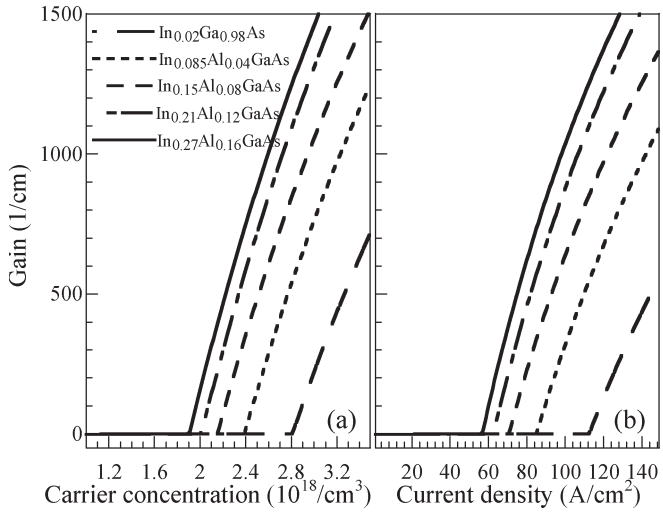

Fig. 5. Peak material gain as a function of (a) carrier concentration and (b) radiative current density of the $In_{0.02}Ga_{0.98}As$ and InAlGaAs QWs with $Al_{0.3}Ga_{0.7}As$ barrier at 95 °C.

in numerical calculations, it is noteworthy that increase of In and Al concentrations will result in a larger amount of strain in InAlGaAs QW and a higher strain level in QW may have crystal quality concerns. Thus, the In and Al concentrations in InAlGaAs QWs cannot be too high. In fact, degradation in higher Al content QW PL has been experimentally observed. Therefore, the $In_{0.15}Al_{0.08}Ga_{0.77}As/Al_{0.3}Ga_{0.7}As$ with a compressive strain of 1.053% is chosen and grown to form the QW active region of the 850-nm VCSEL. The temperature-dependent PL of the $In_{0.15}Al_{0.08}Ga_{0.77}As$ triple-QW structure is shown in Fig. 6. The QW was grown by low pressure MOCVD on GaAs (100) substrate with group-V precursors of arsine (AsH_3). Trimethyl (TM-) sources of aluminum (Al), gallium (Ga), and indium (In) were used for group-III precursors. The thickness of QW is 7 nm, which is identical to that used in numerical calculation. The thickness and Al composition of barriers are 8 nm and 0.3, respectively. The growth rate is about 0.75 nm/s, and the growth temperature is 720 °C. The composition in QW is characterized by the rocking curve of high-resolution X-ray diffraction. Temperature-dependent PL measurement is performed by a 325-nm He–Cd laser with a 20-mW output over the temperature range of 17–300 K. The laser power is 20 mW, and the spot size is about 100 μm in diameter. Luminescence is analyzed by a 320-mm grating monochromator and detected by a charge couple detector.

In Fig. 6, the dots represent the peak emission wavelength obtained from PL measurement, and the curve represents the numerical spontaneous emission rate of the $In_{0.15}Al_{0.08}Ga_{0.77}As/Al_{0.3}Ga_{0.7}As$ QW, which is obtained when the input carrier concentration is 5×10^{15} cm^{-3}, which is calculated based on the excited power density and laser spot size. The peak emission wavelength at 300 K is 838 nm,

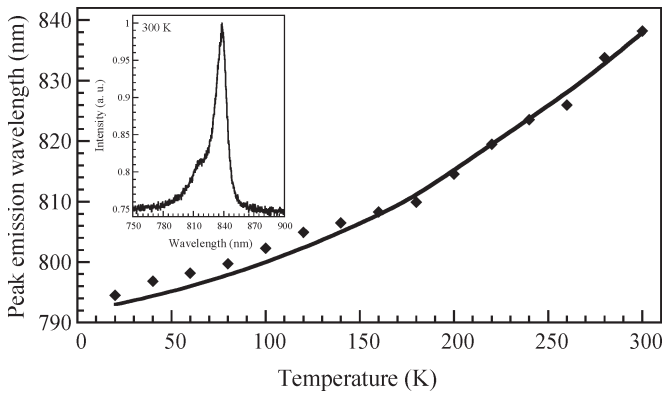

Fig. 6. Temperature-dependent PL peak emission wavelength of the $In_{0.15}Al_{0.08}Ga_{0.77}As$ triple-QW structure. The inset is the optical spectrum obtained at 300 K.

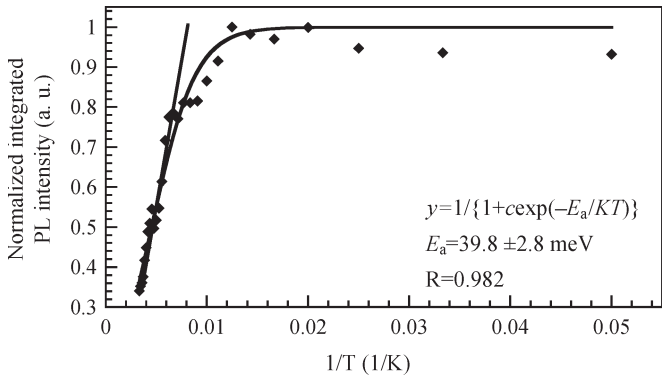

Fig. 7. Normalized integrated PL intensity plotted as a function of reciprocal temperature for the $In_{0.15}Al_{0.08}Ga_{0.77}As$ triple-QW structure.

and the full-width at half-maximum (FWHM) is 13.5 nm, which is comparable to the (In)GaAs/AlGaAs material systems. When the temperature decreases to 20 K, the peak emission wavelength shifts to 793 nm with an FWHM of 6.6 nm. Fig. 7 shows the normalized integrated PL intensity plotted as a function of reciprocal temperature for the $In_{0.15}Al_{0.08}Ga_{0.77}As$ triple-QW structure. Fitting our data to the classical Arrhenius law, $I = I_0/1 + c\,\exp(-E_a/KT)$, according to the thermal carrier transfer mechanism, the activation energy (E_a) of the $In_{0.15}Al_{0.08}Ga_{0.77}As$ QW is determined to be 39.8 meV.

As investigated in the numerical discussion, it is observed that the InAlGaAs QWs can provide a lower transparency carrier concentration and a higher differential gain. The transparency carrier concentration of the InAlGaAs QWs increased with elevated temperature up to 95 °C is also less sensitive than the $In_{0.02}Ga_{0.98}As$ QW. However, more than 20% increment of the transparency carrier concentration is too high to be ignored for the InAlGaAs QWs. Therefore, methods for reduction of temperature sensitivity need to be sought. To reduce the electronic leakage current and the temperature sensitivity of semiconductor lasers, a high-bandgap layer is regularly embedded into the active region before the growth of p-type layers [27]–[29]. In this paper, we propose to employ an AlGaAs electronic blocking layer to improve the high-temperature performance for the 850-nm VCSELs under study.

The schematic diagrams of the VCSEL with a high-bandgap 10-nm-thick $Al_{0.75}Ga_{0.25}As$ electronic blocking layer

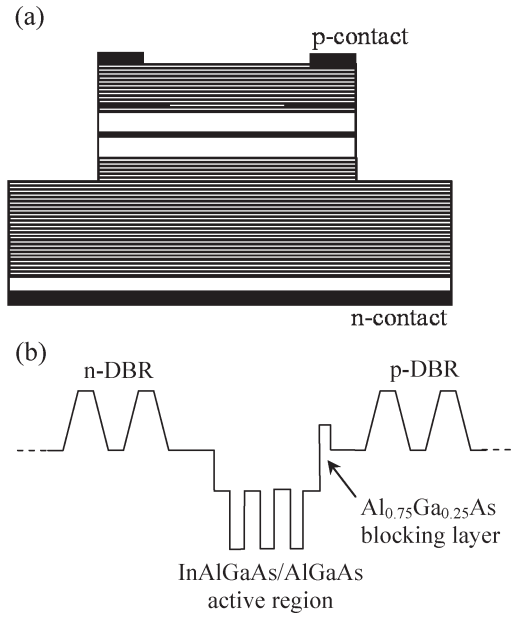

Fig. 8. Schematic diagrams of the VCSEL with employing a high-bandgap $Al_{0.75}Ga_{0.25}As$ electronic blocking layer. (a) Sketch of the fabricated VCSEL structure. (b) Schematic plot of the energy band diagram near the $In_{0.15}Al_{0.08}Ga_{0.77}As/Al_{0.3}Ga_{0.7}As$ active region.

are shown in Fig. 8. In this discussion, the active region of the VCSEL, which was surrounded by $Al_{0.6}Ga_{0.4}As$ spacers to form a one-wavelength cavity, consisted of three 7-nm-thick $In_{0.15}Al_{0.08}Ga_{0.77}As$ QWs and four 8-nm-thick $Al_{0.3}Ga_{0.7}As$ barriers. The n-type and p-type distributed Bragg reflectors (DBRs) consisted of 39 and 21 pairs of $Al_{0.15}Ga_{0.85}As/Al_{0.9}Ga_{0.1}As$, respectively. The dopant sources were SiH_4 and CBr_4. A 30-nm-thick $Al_{0.97}Ga_{0.03}As$ was introduced in the upper cavity spacer layer to form the oxide confinement. Finally, a one-wavelength-thick current-spreading layer and a heavily doped GaAs $(p = 2 \times 10^{19}\ cm^{-3})$ contact layer were grown to complete the structure. The growth temperature of the n-type DBR and the active region were 720 °C, and that of the p-type DBR was 670 °C.

The fabrication process began from depositing a 1.3-μm-thick SiN_x layer, which acted as a hard mask in the following process, onto the wafer by plasma-enhanced chemical vapor deposition (PECVD) at 300 °C. Standard photolithography and reactive ion etching (RIE) using SF_6 with a flow rate of 20 sccm as etching gas were then performed to define the etching pattern on the hard mask. Trench mesa etching by Cl_2 with a flow rate of 2 sccm and Ar plasma were performed to transfer the mask pattern onto the wafer. The etching depth was cautiously controlled to penetrate the active region, and the 30-nm-thick $Al_{0.97}Ga_{0.03}As$ aperture layer was exposed for selective oxidation in 400 °C stream environment. The mesa diameter was 22 μm and the oxide aperture was 7 μm. After oxidation, the residual dielectric was removed, and a second 150-nm-thick SiO_2 by PECVD was deposited for passivation, followed by a partially etched process for contact window. Ti (30 nm)/Pt (50 nm)/Au (200 nm) were deposited onto the heavily p-doped GaAs contact layer for p-contact, and AuGe (50 nm)/Ni (20 nm)/Au (350 nm) were deposited for n-contact.

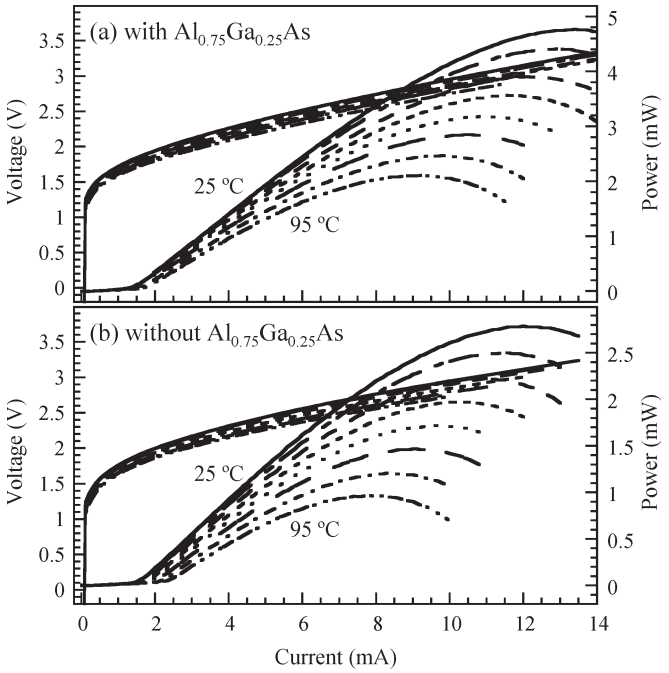

Fig. 9. Temperature-dependent light output and voltage versus current $(L-I-V)$ characteristics of the fabricated VCSELs (a) with and (b) without the high-bandgap $Al_{0.75}Ga_{0.25}As$ electronic blocking layer when the substrate temperature is in the range of 25–95 °C. The step of the temperature increment is 10 °C.

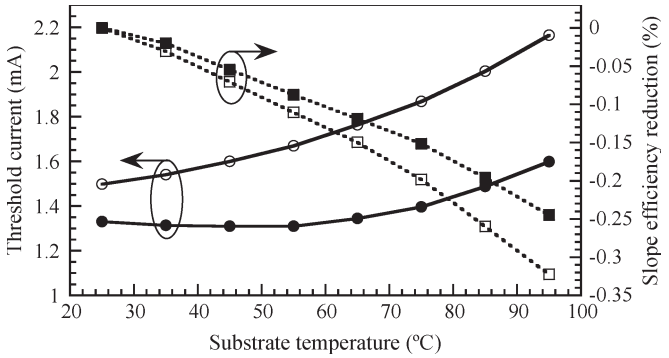

Fig. 10. Threshold current and slope efficiency reduction of the VCSELs with and without the high-bandgap $Al_{0.75}Ga_{0.25}As$ electronic blocking layer as a function of the substrate temperature. Solid and open symbols represent the characteristics of the VCSELs with and without the $Al_{0.75}Ga_{0.25}As$, respectively. The circle and square symbols are for the threshold current and slope efficiency reduction, respectively.

IV. Devices Characteristics

Fig. 9 shows the temperature-dependent light output and voltage versus current $(L-I-V)$ characteristics of the fabricated VCSELs (a) with and (b) without the high-bandgap $Al_{0.75}Ga_{0.25}As$ electronic blocking layer when the substrate temperature is in the range of 25–95 °C. Fig. 10 summarizes the threshold current and slope efficiency reduction of the VCSELs with and without the $Al_{0.75}Ga_{0.25}As$ as a function of the substrate temperature. Solid and open symbols represent the characteristics of the VCSELs with and without the $Al_{0.75}Ga_{0.25}As$, respectively. The circle and square symbols are for the threshold current and slope efficiency reduction, respectively. It is noteworthy that both the gain–cavity detunings

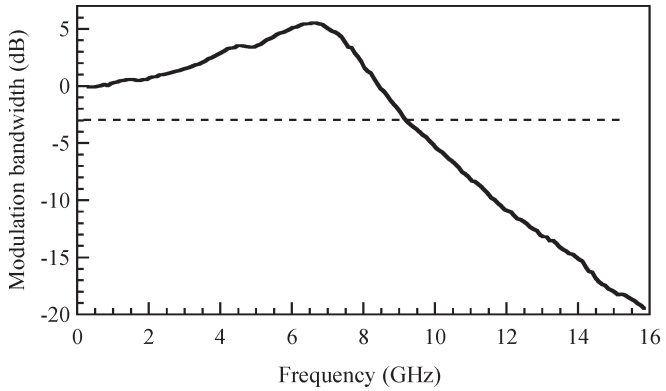

Fig. 11. Small-signal frequency response of the 7-μm-wide VCSEL with $Al_{0.75}Ga_{0.25}As$ layer biased at 4 mA.

of the VCSELs with and without the $Al_{0.75}Ga_{0.25}As$ layer are designed to be 12 nm. The dip of Fabry–Pérot is at 850 nm, which is determined by the reflection measurement. For the VCSEL with $Al_{0.75}Ga_{0.25}As$, the threshold current and slope efficiency at 25 °C are 1.33 mA and 0.53 W/A, respectively. The maximum output power with a 7-μm-wide oxide aperture is 4.8 mW. The amount of increase in threshold current at an elevated temperature of 95 °C is only 0.27 mA, and the slope efficiency drops by only 24.5%. The threshold current and slope efficiency of the VCSEL without $Al_{0.75}Ga_{0.25}As$ at 25 °C are 1.47 mA and 0.37 W/A, respectively, and the threshold current increases to 2.17 mA with a slope efficiency reduction of 32% when the substrate temperature is raised to 95 °C.

The differential resistances of the VCSELs with and without $Al_{0.75}Ga_{0.25}As$ are 102 and 95 Ω, respectively. The small differential resistance may be attributed to the reason that it is more difficult for the carriers to transport in the vertical direction of the VCSEL when the high-bandgap $Al_{0.75}Ga_{0.25}As$ is present. However, it is evident that the temperature sensitivity of the VCSEL with a high-bandgap $Al_{0.75}Ga_{0.25}As$ layer is apparently reduced. Because the effective mass of electrons is smaller than that of holes, the use of a high-bandgap $Al_{0.75}Ga_{0.25}As$ layer can block electrons from overflowing to the p-type layers, and, therefore, the high-temperature characteristics and the output performance of 850-nm $In_{0.15}Al_{0.08}Ga_{0.77}As/Al_{0.3}Ga_{0.7}As$ VCSELs are improved.

Fig. 11 shows the small-signal frequency response of the 7-μm-wide VCSEL with $Al_{0.75}Ga_{0.25}As$ layer biased at 4 mA. The small-signal response of the VCSEL is measured using a calibrated vector network analyzer (Agilent 8720ES) with on-wafer probing and 50-μm multimode optical fiber connected to a New Focus 25-GHz photodetector. The 3-dB modulation frequency response is measured to be $\sim$ 9.2 GHz when the bias current is 4 mA. It is found that the modulation frequency response remains unchanged when the high-bandgap $Al_{0.75}Ga_{0.25}As$ layer is employed in the VCSEL.

V. Conclusion

In summary, the gain-carrier characteristics of the $In_{0.02}Ga_{0.98}As$ and InAlGaAs QWs with 838 nm emission are theoretically investigated. The numerical results suggest that

the incorporation of Al into InGaAs QW is found to provide higher material gain, lower transparency carrier concentration, and radiative current density due to the increment of the amount of strain and the reduced density of states. The optical properties of $In_{0.15}Al_{0.08}Ga_{0.77}As$ QW are also investigated by temperature-dependent PL. With the use of a high-bandgap 10-nm-thick $Al_{0.75}Ga_{0.25}As$ layer in the $In_{0.15}Al_{0.08}Ga_{0.77}As/Al_{0.3}Ga_{0.7}As$ QW active region, the high-temperature characteristics and the output performance are beneficially improved. Small-signal frequency response shows that these VCSELs can provide a modulation bandwidth of approximately 9.2 GHz.

ACKNOWLEDGMENT

The authors thank Dr. I. H. Tan of JDS Uniphase Corporation, Dr. L. H. Laih of M-comm Corporation, and F. I. Lai of the National Chiao-Tung University for useful discussion and technical support.

REFERENCES

[1] J. Gilor, I. Samid, and D. Fekete, "Threshold current density reduction of strained AlInGaAs quantum-well laser," *IEEE J. Quantum Electron.*, vol. 40, no. 10, pp. 1355–1364, Oct. 2004.

[2] J. A. Lehman, R. A. Morgan, M. K. Hibbs-Brenner, and D. Carlson, "High-frequency modulation characteristics of hybrid dielectric/AlGaAs mirror single-mode VCSELs," *Electron. Lett.*, vol. 31, no. 15, pp. 1251–1252, Jul. 1995.

[3] K. L. Lear, A. Mar, K. D. Choquette, S. P. Kilcoyne, R. P. Schneider, Jr., and K. M. Geib, "High-frequency modulation of oxide confined vertical cavity surface emitting lasers," *Electron. Lett.*, vol. 32, no. 5, pp. 457–458, Feb. 1996.

[4] F. H. Peters and M. H. MacDougal, "High-speed high-temperature operation of vertical-cavity surface-emitting lasers," *IEEE Photon. Technol. Lett.*, vol. 13, no. 7, pp. 645–647, Jul. 2001.

[5] T. E. Sale, C. Amano, Y. Ohiso, and T. Kurokawa, "Using strained $(Al_xGa_{1-x})_yIn_{1-y}As_zP_{1-z}$ system materials to improve the performance of 850 nm surface- and edge-emitting lasers," *Appl. Phys. Lett.*, vol. 71, no. 8, pp. 1002–1004, Aug. 1997.

[6] H. C. Kuo, Y. H. Chang, F. Y. Lai, T. H. Hseuh, L. T. Chu, and S. C. Wang, "High speed performance of 850 nm silicon-implanted AlGaAs/GaAs vertical cavity emitting laser," *Solid State Electron.*, vol. 48, no. 3, pp. 483–485, Mar. 2004.

[7] J. Ko, E. R. Hegblom, Y. Akulova, B. J. Thibeault, and L. A. Coldren, "Low-threshold 840-nm laterally oxidized vertical-cavity lasers using AlInGaAs–AlGaAs strained active layers," *IEEE Photon. Technol. Lett.*, vol. 9, no. 7, pp. 863–865, Jul. 1997.

[8] O. Tadanaga, K. Tateno, H. Uenohara, T. Kagawa, and C. Amano, "An 850-nm InAlGaAs strained quantum-well vertical-cavity surface-emitting laser grown on GaAs (311)B substrate with high-polarization stability," *IEEE Photon. Technol. Lett.*, vol. 12, no. 8, pp. 942–944, Aug. 2000.

[9] S. L. Yellen, R. G. Waters, A. H. Shepard, J. A. Baumann, and R. J. Dalby, "Reliability of InAlGaAs strained-quantum-well lasers operating at 0.81 μm," *IEEE Photon. Technol. Lett.*, vol. 4, no. 8, pp. 829–831, Aug. 1992.

[10] N. Tansu, D. Zhou, and L. J. Mawst, "Low-temperature-sensitivity, compressively strained InGaAsP-active ($\lambda = 0.78-0.85$ μm) region diode lasers," *IEEE Photon. Technol. Lett.*, vol. 12, no. 6, pp. 603–605, Jun. 2000.

[11] L. J. Mawst, S. Rulsi, A. Al-Muhanna, and J. K. Wade, "Short-wavelength (0.7 μm $< \lambda <$ 0.78 μm) high-power InGaAsP-active diode lasers," *IEEE J. Sel. Topics Quantum Electron.*, vol. 5, no. 3, pp. 785–791, May/Jun. 1999.

[12] H. K. Choi and C. A. Wang, "InGaAs/AlGaAs strained single quantum well diode lasers with extremely low threshold current density and high efficiency," *Appl. Phys. Lett.*, vol. 57, no. 4, pp. 321–323, Jul. 1990.

[13] T. R. Chen, B. Zhao, L. Eng, Y. H. Zhoung, J. O'Brien, and A. Yariv, "Very high modulation efficiency of ultralow threshold current single quantum well InGaAs lasers," *Electron. Lett.*, vol. 29, no. 17, pp. 1525–1526, Aug. 1993.

[14] N. Tansu and L. J. Mawst, "Compressively-strained InGaAsP-active ($\lambda = 0.85$ μm) VCSELs," in *IEEE Lasers and Electro-Optics Society Annu. Meeting (LEOS)*, Rio Grande, PR, 2000, vol. 2, pp. 724–725.

[15] H. C. Kuo, Y. S. Chang, F. I. Lai, and T. H. Hsueh, "High speed modulation of 850-nm InGaAsP/InGaP strain-compensated VCSELs," *Electron. Lett.*, vol. 39, no. 14, pp. 1051–1052, Jul. 2003.

[16] Y. S. Chang, H. C. Kuo, F. I. Lai, Y. A. Chang, C. Y. Lu, L. W. Laih, and S. C. Wang, "Fabrication and characteristics of high-speed oxide-confined VCSELs using InGaAsP–InGaP strain-compensated MQWs," *J. Lightw. Technol.*, vol. 22, no. 12, pp. 2828–2833, Dec. 2004.

[17] H. K. Choi, C. A. Wang, D. F. Kolesar, R. L. Aggrawal, and J. N. Walpole, "High-power, high-temperature operation of AlInGaAs–AlGaAs strained single-quantum-well diode lasers," *IEEE Photon. Technol. Lett.*, vol. 3, no. 10, pp. 857–859, Oct. 1991.

[18] N. A. Hughes, J. C. Connolly, D. B. Gilbert, and K. B. Murphy, "AlInGaAs/AlGaAs strained quantum-well ridge waveguide lasers grown by metal–organic chemical vapor deposition," *IEEE Photon. Technol. Lett.*, vol. 4, no. 2, pp. 113–115, Feb. 1992.

[19] S. L. Chuang, "Efficient band-structure calculations of strained quantum wells," *Phys. Rev. B, Condens. Matter*, vol. 43, no. 12, pp. 9649–9661, Apr. 1991.

[20] I. Vurgaftman, J. R. Meyer, and L. R. Ram-Mohan, "Band parameters for III–V compound semiconductors and their alloys," *J. Appl. Phys.*, vol. 89, no. 11, pp. 5815–5875, Jun. 2001.

[21] S. Adachi, "Band gaps and refractive indices of AlGaAsSb, GaInAsSb, and InPAsSb: Key properties for a variety of the 2–4 μm optoelectronic device applications," *J. Appl. Phys.*, vol. 61, no. 10, pp. 4869–4876, May 1987.

[22] J. C. L. Yong, J. M. Rorison, and I. H. White, "1.3-μm quantum-well InGaAsP, AlGaInAs, and InGaAsN laser material gain: A theoretical study," *IEEE J. Quantum Electron.*, vol. 38, no. 12, pp. 1553–1564, Dec. 2002.

[23] K. M. Lau, "Ultralow threshold quantum well lasers," in *Quantum Well Laser*, P. Zory, Ed. San Diego, CA: Academic, 1993.

[24] D. Ahn, S. L. Chuang, and Y. C. Chang, "Valence-band mixing effects on the gain and the refractive index change of quantum-well lasers," *J. Appl. Phys.*, vol. 64, no. 8, pp. 4056–4064, Oct. 1988.

[25] S. Seki, H. Oohashi, H. Sugiura, T. Hirono, and K. Yokoyama, "Study on the dominant mechanisms for the temperature sensitivity of threshold current in 1.3 μm InP-based strained-layer quantum-well lasers," *IEEE J. Quantum Electron.*, vol. 32, no. 8, pp. 1478–1486, Aug. 1996.

[26] J. W. Pan and J. I. Chyi, "Theoretical study of the temperature dependence of 1.3 μm AlGaInAs–InP multiple-quantum-well lasers," *IEEE J. Quantum Electron.*, vol. 32, no. 12, pp. 2133–2138, Dec. 1996.

[27] G. B. Stringfellow and M. G. Craford, *High Brightness Light Emitting Diodes*. San Diego, CA: Academic, 1997.

[28] S. Nakamura, M. Senoh, S. Nagahama, N. Iwasa, T. Matsushita, and T. Mukai, "Blue InGaN-based laser diodes with an emission wavelength of 450 nm," *Appl. Phys. Lett.*, vol. 76, no. 1, pp. 22–24, Jan. 2000.

[29] Y. K. Kuo and Y. A. Chang, "Effect of electronic current overflow and inhomogeneous carrier distribution on InGaN quantum well laser performance," *IEEE J. Quantum Electron.*, vol. 40, no. 5, pp. 437–444, May 2004.

Yi-An Chang was born in Taipei, Taiwan, R.O.C., on March 13, 1978. He received the B.S. and M.S. degrees in physics from the National Changhua University of Education (NCUE), Changhua, Taiwan, in 2001 and 2003, respectively. He is currently working toward the Ph.D. degree at the Institute of Electro-Optical Engineering, National Chiao-Tung University, Hsinchu, Taiwan.

He joined the Laboratory of Lasers and Optical Semiconductors at NCUE in 2000 where he was engaged in research on passive Q-switching with solid-state saturable absorbers and III-nitride semiconductor materials for light-emitting diodes and semiconductor lasers under the instruction of Prof. Y.-K. Kuo. His recent research interests include III-nitride and InGaAsN semiconductor devices and infrared vertical-cavity surface-emitting lasers (VCSELs) under the instruction of Prof. H.-C. Kuo and Prof. S.-C. Wang.

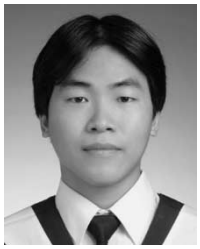

Jun-Rong Chen was born in Taichung, Taiwan, R.O.C., on October 23, 1980. He received the B.S. degree in physics from the National Changhua University of Education (NCUE), Changhua, Taiwan, in 2004. He is currently working toward the M.S. degree in optoelectronics at the Institute of Photonics, NCUE.

He joined the Laboratory of Lasers and Optical Semiconductors at NCUE in 2002, where he was engaged in research on III–V semiconductor materials for light-emitting diodes, organic light-emitting diodes (OLEDs), and semiconductor lasers under the instruction of Prof. Y.-K. Kuo. His recent research interests include III-nitride semiconductor lasers, 850-nm vertical-cavity surface-emitting lasers, and OLED.

Hao-Chung Kuo (S'98–M'99) received the B.S. degree in physics from the National Taiwan University, Taipei, Taiwan, R.O.C., in 1990, the M.S. degree in electrical and computer engineering from Rutgers University, New Brunswick, NJ, in 1995, and the Ph.D. in electrical and computer engineering from the University of Illinois-Urbana Champaign in 1999.

He has an extensive professional career, both in research and industrial research institutions, which includes the following: Research Consultant in Lucent Technologies, Bell Labs (1995–1997); R&D Engineer in the Fiber-Optics Division at Agilent Technologies (1999–2001); and R&D Manager in LuxNet Corporation (2001–2002). In 2002, he joined the National Chiao-Tung University as a Faculty member of the Institute of Electro-Optical Engineering. His current research interests include the epitaxy, design, fabrication, and measurement of high-speed InP- and GaAs-based vertical-cavity surface-emitting lasers, as well as GaN-based light-emitting devices and nanostructures. He has authored or coauthored over 60 publications.

Yen-Kuang Kuo was born in Chia-Yi, Taiwan, R.O.C., on July 19, 1959. He received the B.S. degree in electrophysics from National Chiao-Tung University, Hsin Chu, Taiwan, in 1982, the M.S. degree in electrical engineering from the National Taiwan University, Taipei, Taiwan, in 1984, and the Ph.D. degree in electrical engineering from the University of Southern California (USC), Los Angeles, in 1994.

From 1984 to 1991, he was with the Aeronautical Research Laboratory, Chung Shan Institute of Science and Technology, Taichung, Taiwan. He was a Postdoctoral Research fellow at the Center for Laser Studies, USC, from 1994 to 1995, where he was engaged in research on passive Q-switching with solid-state saturable absorbers. From 1995 to 1997, he was with the Aerospace Industrial Development Corporation, Taichung. In 1997, he joined the faculty of the Department of Physics, National Changhua University of Education, Changhua, Taiwan, where he is a Professor at the Department of Physics and Institute of Photonics, and the Head of the Laboratory of Lasers and Optical Semiconductors. His recent research interests include passive Q-switching with solid-state saturable absorbers and semiconductor materials for light-emitting diodes, organic light-emitting diodes, and semiconductor lasers.

Shing-Chung Wang (M'79–SM'03) received the B.S. degree from the National Taiwan University, Taipei, Taiwan, R.O.C., the M.S. degree from the National Tohoku University, Sendai, Japan, and the Ph.D. from Stanford University, Stanford, CA, in 1971, all in electrical engineering.

He has an extensive professional career, both in academic and industrial research institutions, which includes the following: Faculty member at the National Chiao-Tung University (1965–1967); Research Associate at Stanford University (1971–1974); Senior Research Scientist at Xerox Corporation (1974–1985); and Consulting Scientist at Lockheed-Martin Palo Alto Research Laboratories (1985–1995). In 1995, he rejoined the National Chiao Tung University as a Faculty member of the Institute of Electro-Optical Engineering. His current research interests include semiconductor lasers, vertical-cavity surface-emitting lasers, blue and ultraviolet (UV) lasers, quantum-confined optoelectronic structures, optoelectronic materials, diode-pumped lasers, and semiconductor laser applications. He has authored or coauthored over 160 publications.

Prof. Wang is a Fellow of the Optical Society of America. He is a recipient of the Outstanding Scholar Award from the Foundation for the Advancement of Outstanding Scholarship.